Suomi-NPP VIIRS Ice Surface Temperature Algorithm Theoretical Basis Document (ATBD)

Science Principal Investigator: Dr. Mark Tschudi

Correspondence e-mail address: mark.tschudi@colorado.edu

Prepared by Mark Tschudi, George Riggs, Dorothy Hall, and Miguel O. Román

Version 1.0

13 January 2016

Table of Contents

1.0 Introduction

Ice Surface Temperature (IST) is a crucial measure of the Arctic climate, as it is an important indicator of the energy balance at the ice surface. The Suomi-NPP (S-NPP) Visible Infrared Imaging Radiometer Suite (VIIRS) IST has been developed to map sea ice surface temperature regionally and globally (Figure 1).
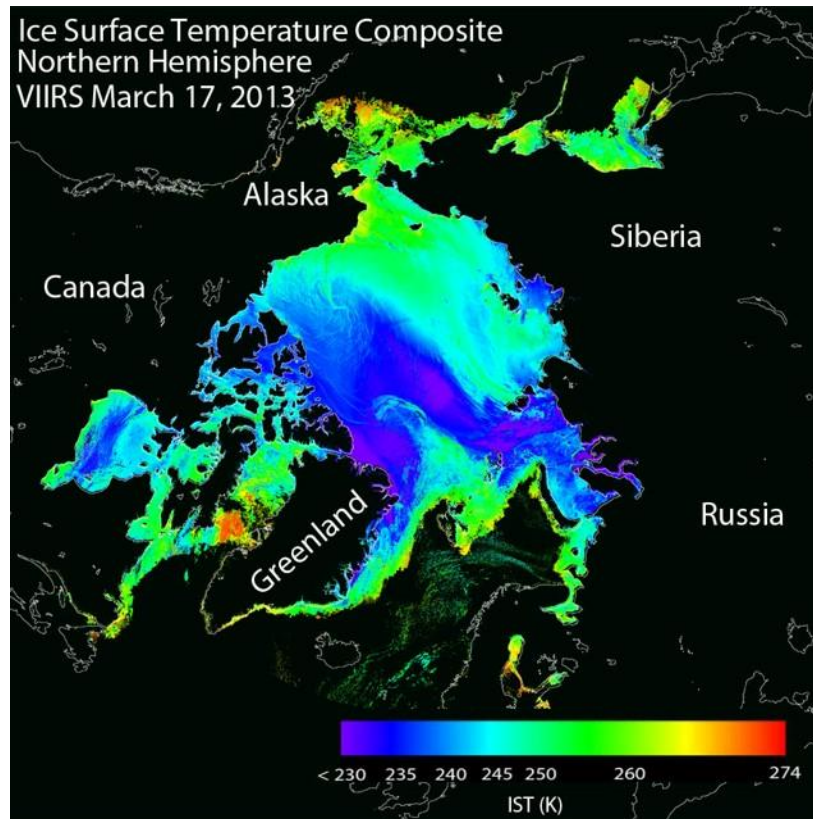

Figure 1: IDPS VIIRS IST in the Northern Hemisphere, March 17, 2013. Cloud mask has not been applied. By D. Baldwin, U. of Colorado, Boulder.

The VIIRS IST product provides the radiating or "skin" temperature at the sea ice surface. IST is the aggregate temperature of objects comprising the ice surface, including snow and melt water on the ice. IST serves as an excellent indicator of freeze/thaw processes on ice, and has been used to separate thin ice from open water. It also provides coverage of sea ice during polar night, in higher resolution than passive microwave sensors. The VIIRS IST algorithm uses calibrated radiance data from two VIIRS thermal infrared channels in a split-window technique to estimate IST. The heritage Moderate Resolution Imaging Spectroradiometer (MODIS) IST algorithm is used as the foundation for the VIIRS IST algorithm. The NASA VIIRS IST product format has been updated from the MODIS Sea Ice Extent and IST product [*Hall et al.*, 2001], with the VIIRS IST product now being stand-alone, and VIIRS daytime sea ice extent as a separate product. The theory of the split window technique for IST derivation is discussed, followed by a description of the algorithm and data product. The accuracy and uncertainty of the

algorithm and product, and validation approach are then presented. Information on the data product format is also given.

1.1 Science/Applications Rationale for the Product

The Arctic sea ice environment is rapidly changing [*Meier et al.*, 2014]. Areal coverage of sea ice is decreasing at a significant rate over the modern (since 1979) satellite record and appears to have accelerated over the past decade [e.g., *Cavalieri et al.*, 2012; *Comiso and Nishio*, 2008], particularly during summer, with record low minimum extents in the past several years [e.g., *Parkinson and Comiso*, 2013]. For September, the time of minimum extent, the sea ice extent has been decreasing by 13%/year, with the lowest 9 extents witnessed during the last 9 years (*NSIDC*, 2015; Figure 1). Recent satellite data have also indicated that older [*Maslanik et al.*, 2011; 2007] and thicker [e.g., *Kurtz et al.*, 2011] sea ice has steadily been decreasing.

Figure 1: September Arctic sea ice extent trend. From NSIDC [2015].

IST has a profound influence on sea ice growth, snow metamorphosis, and snow/ice melt [*Key et al.*, 1997]. IST and sea ice thickness are viewed as the most important parameters affecting sea ice from a thermodynamic perspective [*Bitz and Lipscomb*, 1999]. IST is used, among other factors, to compute ice thickness in a one-dimensional sea ice thickness model [*Wang et* al.,

2010]. A long-term data set of IST can be used to detect and understand the timing and duration of the summer melt and ice growth seasons, and freeze/thaw cycles.

For years the collection of IST has relied on in situ measurement from ships, manned ice camps and drifting buoys. Large-scale estimates of IST began in the 1970's and continues to present day, by using thermal channels on board a series of NASA and NOAA satellites. The IST product produced from VIIRS will carry the record forward from MODIS, with a product that has improved calibration and spatial resolution.

1.2 Intended user community

The VIIRS IST product provides a data record of the evolution of IST over sea ice poleward of 50°N and 50°S latitude throughout the year, during daytime and nighttime periods [*Justice et al*., 2013; *Key et al*., 2013]. Users of IST products include the U. S. National/Naval Ice Center (NIC), Naval Research Laboratory, and the Alaska Ice Desk of the National Weather Service, and various university and government researchers. The IST algorithm and data products will extend the Earth Observing System (EOS) IST data product record. The heritage NASA EOS MODIS IST data record, which began in 2000 and is ongoing, has been used for research to determine IST impact on sea ice formation and melt, and estimation of thin sea ice thickness (see Section 2.1).

2.0 Algorithm Description

The NASA VIIRS IST algorithm calculates IST over sea ice using a split window statistical regression method, employing two VIIRS thermal bands, with refinement of the empircal coefficients achieved via comparisons with ancillary data. The theory of the split-window technique is discussed, along with limitations, sources of error and implementation of the IST algorithm in the following sections.

2.1 Technical Background and Heritage

Satellite-based IST was first derived using thermal infrared channels available through the Advanced Very High Resolution Radiometer (AVHRR). Several studies compared estimated IST from AVHRR with in-situ measurements [*Key et* al., 1997; *Yu et al.,* 1995; *Lindsay and Rothrock*, 1994; *Key and Haeflinger*, 1994; 1992]. AVHRR IST observations have also been utilized to estimate thin ice thickness in leads [*Yu and Lindsay*, 2003; *Yu and Rothrock,* 1996]. The 2003 study concluded that thin ice estimates using IST were accurate when compared to thickness derived from the RADARSAT Geophysical Processor System (RGPS), although difficulties with AVHRR thickness estimates occurred in regions with major ice deformation. *Tschudi et al.* [2010] tracked AVHRR IST evolution on sea ice parcels as they advected through the Arctic Ocean. The algorithm for retrieval of IST from AVHRR was later adopted for MODIS by *Hall et al*. [2004; 2001], using the techniques of *Key et al*. [1997]. *Hall et* al. [2001] validated the technique for computing the MODIS IST by examining imagery from the MODIS Airborne Simulator.

Recent studies have utilized satellite-derived IST products to examine timing and duration of sea ice freeze-up and melt. For example, in a regional study by *Ciappa et al.* [2012], the MODIS heritage IST product was analyzed to investigate changes in the Terra Nova Bay polynya. The MODIS IST product has also been used to obtain information about the recent rapid melting of Arctic sea ice by *Kang et al.* [2014]. Their results suggest a statistically significant relationship between the IST maximum, along with wind vorticity, during June–July and the sea ice extent minimum in September (Figure 2). MODIS IST has also been examined to determine the variability in IST and melt extent over the Greenland Ice Sheet [*Hall et al.*, 2013].
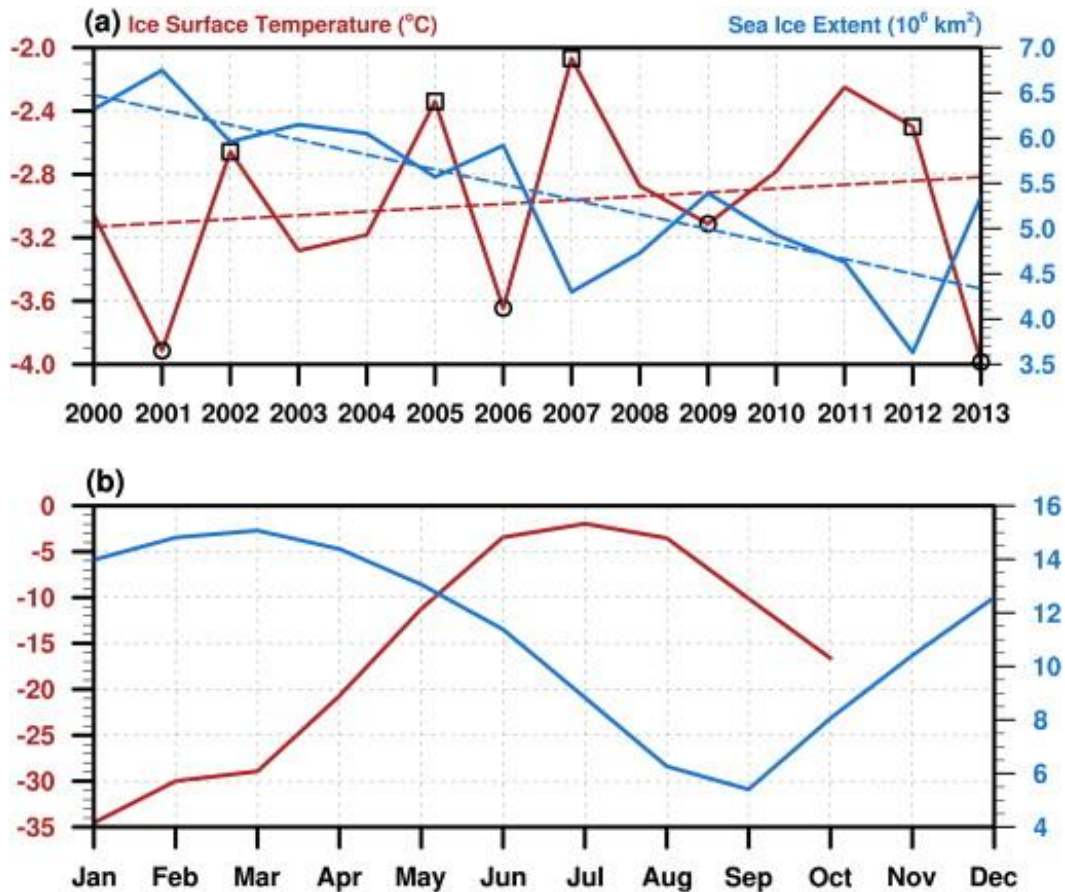

Figure 2: (a) Time series of IST in JJA (red) and sea ice extent in September (blue). Dashed lines indicate linear trend of each variable (solid lines). And (b) Monthly mean IST (red) and sea ice extent (blue) obtained over 14 years (2000–2013). From Kang et al. [2014].

The VIIRS IST algorithm is an update of the MODIS IST algorithm, replacing MODIS thermal bands with VIIRS thermal bands, and utilizing new empirical coefficients for VIIRS. These coefficients will be periodically tuned using ancillary IST measurements. The VIIRS IST product will utilize the improved technology and spatial resolution of thermal bands for VIIRS (750m, compared to 1km for MODIS).

2.2 VIIRS IST Algorithm Description

Similar to the MODIS IST algorithm by *Hall et al*. [2001], the VIIRS IST algorithm utilizes two thermal IR bands for mapping sea ice surface temperature. Based on previous observations [*Riggs et al.,* 1999], sea ice is identified as ocean areas poleward of 50°N and 50°S that have a surface temperature less than or equal to 271.4K.

The basis of the NASA VIIRS IST algorithm is the work of *Key et al*. [1997], who state that the demonstrated accuracy of the algorithm is sufficient for most climate process studies. The major caveat with the algorithm is that it is applicable only to clear-sky conditions. Inadequate cloud masking may result in significant error in estimating the IST. The heritage of the VIIRS IST algorithm is *Key and Haefliger* [1992] with substantiation of robustness and accuracy by later work [*Key et al.*, 2013, 1994; *Yu et al*., 1995; *Lindsay and Rothrock*, 1994; *Massom and Comiso*, 1994).

To compute the IST from VIIRS band M15 and M16, we use the VIIRS Level 1B data for these thermal channels, which are stored as calibrated radiance data. The calibrated radiance data for VIIR bands M15 and M16 are converted to brightness temperature (*T*), using the method of *Key et al.* [1994], who used an inversion of Plank's equation with an emissivity term:

$$T = c_2\lambda / \ln (1 + (\varepsilon\, c_1\, \lambda^3) / L), \tag{1}$$

where c_1 = 1.1910659 * 10^{-5} mW/m^2 sr cm^{-4}, c_2 = 1.438833 cm K, and λ is the central wavelength (cm) for each band. *L* is the calibrated radiance from the sensor (mW/m^2 sr cm^{-1}) and *e* the emissivity for each band.

Once the brightness temperature *T* has been computed for each band (T11 and T12), the IST is calculated using the split-window method of *Yu et al*. [1995], updated for VIIRS M15 and M16 bands:

$$IST = a + bT11 + c\, (T11 - T12) + d\, [(T11 - T12)\, (secq-1)], \tag{2}$$

where *T11* is the brightness temperature (K) for VIIRS band M15 (10.8µm), *T12* the brightness temperature (K) for VIIRS band M16 (12.0µm), *q* the scan angle from nadir, and *a*, *b*, *c*, *d* are the empirically-determined coefficients that compensate for atmospheric effects, notably humidity.

Initial empirical coefficients were obtained from Dr. J. Key (NOAA-NESDIS) and Dr. Y. Liu (Univ. WI, Madison). Separate sets of the 4 coefficients (*a, b, c, d*) are used for the Arctic and Antarctic, and according to the estimated IST ranges of < 240K, 240K < IST < 260K, and > 260K.

2.2.1 Algorithm Limitations

Though the split window is a robust technique for IST measurement it does have limitations. IST estimates from AVHRR data have exhibited error, mainly due to uncertainty caused by cloud masking and haze [*Lindsay and Rothrock*, 1994]. Sea ice may move relatively rapidly and clouds may obscure this movement or make the movement of the sea ice appear incoherent over short (1 day) time scales. In this regard, cloud masking is one of the biggest challenges for IST estimation from satellite observation [*Wang & Key*, 2005].

In the VIIRS IST product, screening for clouds is accomplished by applying the VIIRS Cloud Mask (VCM) data product [*Godin*, 2014]. The VCM Cloud Detection Results & Confidence Indicator flag is used to mask cloud and cloud contamination from pixels. If that flag is set to "confident cloudy" or "probably cloudy," then the pixel is labeled as cloud obscured in the sea ice map, and IST is not calculated. Analysis of the sea ice product and associated analysis of the cloud mask has revealed that the cloud mask algorithm performance is very different between daylight and darkness. In daylight, the cloud mask has been cloud biased resulting in greater cloud coverage than may exist and identifies sea ice as cloud in many situations. In darkness, the cloud mask has been biased toward identifying clear conditions, resulting in a lack of cloud coverage when there probably is some.

It is recognized that, even under clear-sky conditions, water vapor will affect the accuracy of the IST calculation. There is likely to be more water vapor in the boundary layer when melt ponds and leads are present, but this is handled by the algorithm automatically. The coefficients are primarily used to correct for atmospheric water vapor.

Another difficulty with surface temperature retrieval occurs when melt ponds and leads are present. The emissivity over water will be somewhat lower than that of snow or ice, say 0.96 compared to 0.99. This will make a difference of a few tenths of a degree [Jeff Key, written communication, 1996]. The directional effects are also probably slightly different in melt ponds and leads as compared to snow- or ice-covered sea ice.

Global and regional error analysis of the NASA VIIRS IST product is accomplished with other sources of VIIRS IST, such as the VIIRS Interface Data Processing System (IDPS) IST [*Baker*, 2011] and MODIS IST [*Hall et al.*, 2001] products, as well as IST measured during NASA's Operation IceBridge campaign [*Kurtz et al.*, 2013].

2.2.2 Algorithm Flow

The general flow of the IST algorithm is shown in Figure 3. The algorithm is run for all ocean pixels for VIIRS thermal band swaths poleward of 50°N and 50°S latitude, without restrictions. A land mask is then applied, and a "raw IST" product is computed using (1) and (2) over all ocean pixels and stored. Next, the cloud mask (VCM) is applied, with a fill value assigned for all "confidently cloudy" or "probably cloudy" pixels. An "open ocean" mask is then applied for

all pixels greater than 271.4K, with a second fill value assigned. This modified dataset is then stored in the record. For each pixel, quality flags (QFs) are stored a bit flag array. These QFs are the VCM cloud flag, and M15 and M16 band QFs, which are carried over from the VCM and the thermal band input data respectively. Other QFs produced are the day/night flag (day if solar zenith angle $< 85°$) and an overall QF, which is based on the values of the other QFs.
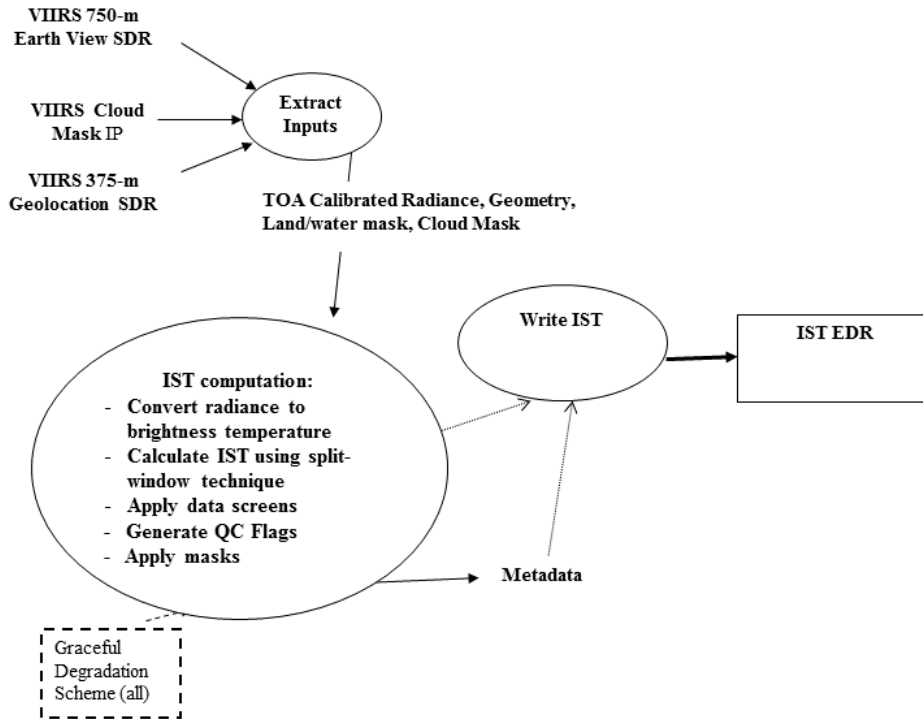

Figure 3: Suomi-NPP VIIRS IST Algorithm Flow Chart.

This algorithm flow is used so that the algorithm is applied under all conditions, allowing the user to examine the "raw" IST data before any masks or screens are applied, except the land mask. The raw data is then screened with the VCM, ocean/ice mask, and stored as a second dataset. For each pixel, QA bit flags are produced so users can determine if the result for a pixel is usable in their research or application.
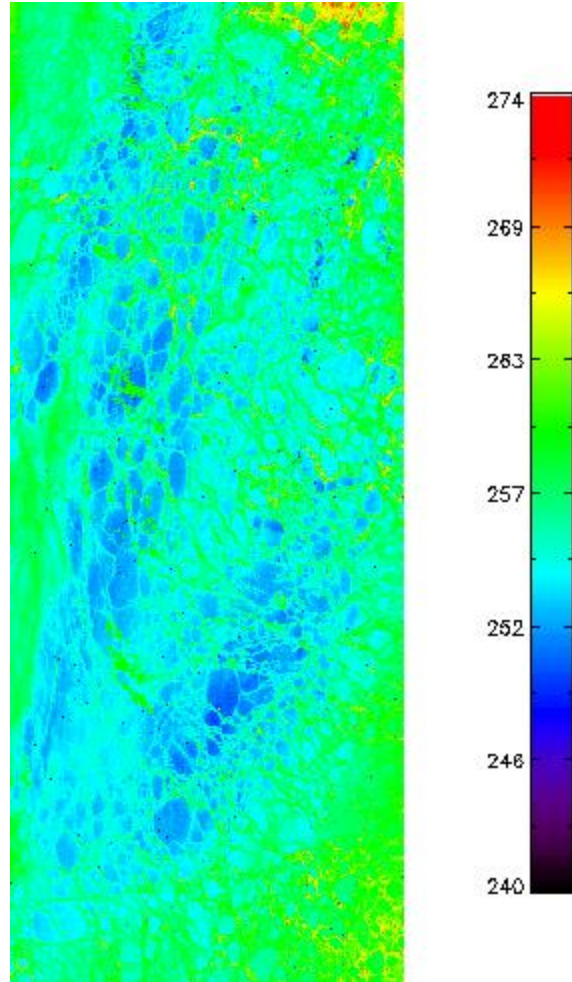
2.3 Product Description

The NASA VIIRS Level-2 IST Product, with Earth Science Data Type name VNP29, will have the following data arrays: Raw IST, Screened IST, and algorithm QA bit flags. Each data array has local attributes describing the data, and the product has global metadata to support archiving and use of the product.

Raw-IST

This IST data array is generated by the IST algorithm and contains all IST values, except in land-masked areas, poleward of 50°N and 50°S. Figure 4 (right) is an example of the raw IST (in Kelvins) from one of our test runs.

Figure 4 (right): "Raw IST," with no cloud mask applied, over the Beaufort Sea on September 12, 2014. From a VIIRS IST test run using the NASA Science Investigator-led Processing System (SIPS). IST is in Kelvins.

Screened-IST

The Screened IST data array is the IST map generated by the algorithm with clouds (VCM) and an ocean mask (>271.4K) overlaid by setting the IST to a fill value corresponding to each mask. IST is represented in Kelvins, with values in the expected range of 213-275K for each pixel.

Quality flag arrays

Quality flags from the VCM, and the input VIIRS thermal bands (M15 and M16) are stored in separate arrays.

Basic Quality flag

A general quality flag is assigned, based on the VCM and VIIRS thermal band flags, as well as whether the data was screened by the land mask or by the ice/ocean mask. This is used to indicate quality ranging from best to poor, to provide a user with a convenient value for initial quality assessment of the data.

Bit flags (QFs)

Algorithm specific bit flags are set in this data array. Bit flags are set for day/night, ocean/land, and cloud/no cloud, which is set to "cloud" if the VCM indicates the pixel is "confidently cloudy" or "probably cloudy." Multiple bit flags may be set. Local attributes describing the data, i.e. each bit flag, are included for the data array.

3.0 Product Inputs

The Land PEATE or Land SIPS IDPS versions of the VIIRS input products have been used for algorithm development and evaluation. The NASA VIIRS products will be used as input when Land SIPS begins operational production of those products. Input Earth Science Data Types (ESDTs) and data arrays (the bit flag used if a bit flag array) are listed in Table 1.

ESDT	Data array names	Nominal spatial resolution	Descriptor
NPP_VMAE_L1	BrightnessTemperature_M15	750 m	TOA
	QF1_VIIRSMBANDSDR_M15		Poor quality flag
	BrightnessTemperature_M16	750 m	TOA
	QF1_VIIRSMBANDSDR_M16		Poor quality flag
	SolarZenithAngle	750 m	Solar zenith angle
	SatelliteZenithAngle	750 m	Satellite zenith angle
NPP_CMIP_L2	QF1_VIIRSCMIP (bits 2-3)	750 m	Cloud mask confidence
	QF2_VIIRSCMIP (bits 0-2)	750 m	Land/water mask

Table 1. VIIRS data product inputs to VNP29_L2 algorithm.

3.1 Spectral Bands

VIIRS VIS, SWIR and thermal bands are used as input. Input ESDTs and spectral bands are listed in Table 2.

ESDT	Data array	wavelength	Nominal spatial resolution
NPP_VMAE_L1	BrightnessTemperature_M15	10.763 µm	750 m
	BrightnessTemperature_M16	12.013 µm	750 m

Table 2. VIIRS spectral band inputs to VNP29_L2 algorithm.

3.2 Masks, Thresholds and Ancillary Data

Several data screens, masks and thresholds are applied in the algorithm to mask clouds, flag uncertain IST detections, and set QA bit flags. Data screens and masks are created within the algorithm with data read from the VIIRS input data products. No ancillary data are used in the algorithm. Data screens and masks used are described next.

Land/Water Mask

The land/water mask is currently read from the IDPS CMIP product (NPP_CMIP_L2). When the NASA VIIRS version of the land/water mask based on the heritage MODIS land/water mask becomes available it will be used in the algorithm because of its heritage. It has more classes and better accuracy than the CMIP land/water mask. The land/water mask is used to mask land and to identify inland water bodies. The VIIRS IST algorithm does not currently perform ice detection in inland waters.

Cloud Mask

Discrimination of cloud from snow on sea ice is very challenging because some types of clouds and snow on sea ice can have very similar reflectance characteristics. The CMIP cloud detection results & confidence indicator is used in the IST algorithm to mask clouds. If the cloud

confidence flag reports "confident cloudy" or "probably cloudy" for a pixel, the pixel is masked as cloud. If a pixel is "confidently clear" or "probably clear," the pixel is processed.

The CMIP is accurate in cloud detection in most situations; however there are some persistent cloud/sea ice confusion problems that appear in the IST product. Some discussion of uncertainty in cloud detection is presented in Sec. 4.0. (Note: when the NASA version of the cloud mask product becomes available it will replace the IDPS CMIP product as the cloud mask input product.)

4.0 Product Accuracy/Uncertainty

Sea ice identification does not have many of the complicating factors of varying surface covers that affect mapping features on land, but there are complications that make sea ice mapping difficult. Because sea ice can vary in concentration from near zero to 100 percent, sea ice can give different IST within a scene, due to mixed-pixel effects. The presence of melt ponds and leads in the summer months will affect the emissivity of the ice surface and therefore the calculation of ice surface temperature.

The accuracy of the IST algorithm for the IDPS VIIRS IST product is approximately 1K [*Key et al*., 2013]. The NASA VIIRS IST accuracy will be similar, and will be assessed via comparisons with the NASA MODIS IST product [*Hall et al*., 2004; 2001] and validated with NASA Operation IceBridge airborne IST measurements [*Krabill and Buzay*, 2012].

Coefficients obtained from *J. Key* and *Y. Liu* [personal communication] are initially used in the NASA VIIRS IST algorithm. The coefficients are based on VIIRS-specific calculations they performed. Further analysis of NASA VIIRS IST evaluations will likely result in changes to the coefficients.

Clouds pose many of the same problems in mapping IST as they do when mapping other surface features, such as snow. Sea ice may move relatively rapidly and clouds may obscure this movement or make the movement of the sea ice appear incoherent when an 8-day time series, partially obscured by clouds, is compiled. Small ice floes, polynyas, and leads at subpixel resolution contribute error to identification and mapping of sea ice. Global error analysis is ongoing with other sources of data, e.g. passive-microwave and regional operational sea ice data products, to estimate error at regional and global scales in the post-launch time period.

4.1 Uncertainty Estimate

The targeted uncertainty of the NASA VIIRS IST product is ±1K over a measurement range of 213-275K. Previous estimation of the IDPS VIIRS IST uncertainty with comparisons to the NASA MODIS IST Product approach this uncertainty overall, but show a greater uncertainty (2-

3K) for warmer IST (>250K) [*Key et al*., 2013], with the VIIRS IST cooler than MODIS. Measurement uncertainty is defined as the root-mean-square of the measurement errors.

4.2 Validation Approach

To validate the product, the uncertainties and accuracy of the NASA VIIRS IST product at the pixel level will be defined via comparisons with airborne IST data from NASA's Operation IceBridge [*Kurtz et al*,. 2013, www.nasa.gov/mission_pages/icebridge/index.html]. This ongoing campaign deploys an aircraft with several instruments, including a Heitronics, Inc. KT-19, which is a downward-pointing, IR pyrometer that measures IST, although no atmospheric corrections are performed [*Krabill and Buzay*, 2012]. Techniques to bin these data into the appropriate VIIRS pixels, and to minimize overpass time and distance differences, have been established for validation of the IDPS VIIRS IST Product (Figure 5). Adjustments to the NASA VIIRS IST algorithm regression coefficients may be made, based on results from this validation. Inter-comparisons of the NASA VIIRS IST with other satellite-derived data products, such as the MODIS IST [*Hall et al*., 2001] and IDPS VIIRS IST [*Baker*, 2011] will also be used to assess the product quality.
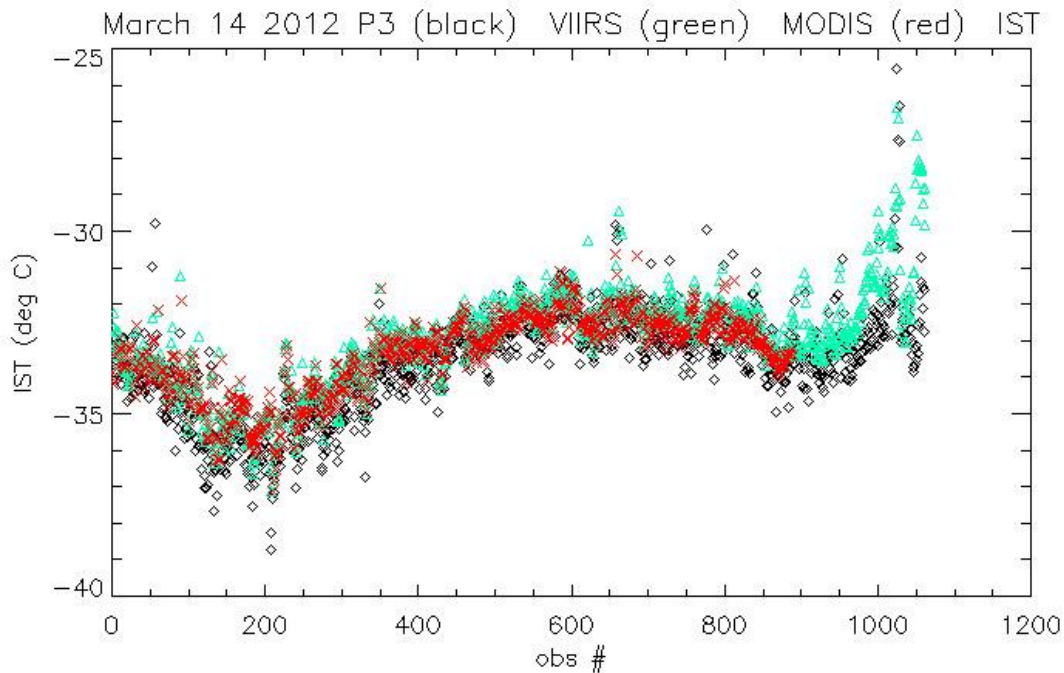

Figure 5: Comparison between the IST (in deg C) measured during IceBridge (black), the nearest IDPS VIIRS IST measurement (green) and MODIS observation (red). Measurements were made on March 12, 2014, over the Arctic Ocean, off the Northwest coast of the Canadian Archipelago.

5.0 Data Format

The data product format will be HDF5.

5.1 Format

The IST data will be stored as data arrays with local attributes describing the data. The product will include metadata relevant to archive, data identification, provenance/processing history and data quality of the product.

5.2 QA Metadata

QA metadata is written as global attributes that provide information on overall summary quality of the product, such as the percentage of good data processed in a swath.

6.0 Product Publications

A NASA VIIRS IST data product user guide will be written and posted at the NSIDC DAAC. The IST product is also referenced in:

Justice, C.O., Román, M.O., Csiszar, I., Vermote, E., Wolfe, R., Hook, S.J., Friedl, M., Wang, Z., Schaaf, C., Miura, T., Tschudi, M., Riggs, G., Hall, D.K., Lyapustin, A., Devadiga, S.,Davidson, C., & Masuoka, E. (2013). Land and Cryosphere Products from Suomi NPP VIIRS: Overview and Status. Journal of Geophysical Research-Atmospheres, 118, 1-13, doi:10.1002/jgrd.50771.

7.0 References

Baker, N. (2011), Joint Polar Satellite System (JPSS) VIIRS Ice Surface Temperature Algorithm Theoretical Basis Document (ATBD), 474-00052, 40 pp., NASA Goddard Space Flight Center, Greenbelt MD.

Bitz, C.M. and Lipscomb, W.H. (1999), An energy-conserving thermodynamic model of sea ice, J. Geophys. Res.,104, C7, DOI: 10.1029/1999JC900100.

Cavalieri, D.J. and Parkinson, C.L. (2012), Arctic sea ice variability and trends, 1979–2010, The Cryosphere, 6, 881-889, doi:10.5194/tc-6-881-2012.

Ciappa, A., L. Pietranera, G. Budillon (2012), Observations of the Terra Nova Bay (Antarctica) polynya by MODIS ice surface temperature imagery from 2005 to 2010. Remote Sensing of Environment, 119 (2012), pp. 158–172.

Comiso, J.C., and F. Nishio (2008), Trends in the sea ice cover using enhanced and compatible AMSR-E, SSM/I, and SMMR data, J. Geophys. Res., 113, C02S07, doi:10.1029/2007JC004257.

Godin, N., (2013), JPSS VIIRS Cloud Mask Algorithm Theoretical Basis Document (ATBD), Rev E, 474-00033, 101 pp., NASA Goddard Space Flight Center, Greenbelt MD.

Hall, D., J.C. Comiso, N.E. DiGirolamo, C.A. Shuman, J.E. Box, and L.S. Koenig. (2013). Variability in the surface temperature and melt extent of the Greenland ice sheet from MODIS, Geophys. Res. Lett., 40, 1-7. doi: 10.1002/grl.50240

Hall D.K., G.A.Riggs and V.V. Salomonson (2001), Algorithm Theoretical Basis Document (ATBD) for the MODIS Snow and Sea Ice-Mapping Algorithms. http://modis-snow-ice.gsfc.nasa.gov/atbd.html.

Hall, D.K., J. Key, K.A. Casey, G.A. Riggs, and D.J. Cavalieri (2004), Sea ice surface temperature product from the Moderate Resolution Imaging Spectroradiometer (MODIS), IEEE Trans. Geosci. Remote Sensing, 42(5), 1076-1087.

Justice, C.O., M. O. Román, I. Csiszar, E. F. Vermote, R. E. Wolfe, S. J. Hook, M. Friedl, Z. Wang, C. B. Schaaf, T. Miura, M. Tschudi, G. Riggs, D. K. Hall, A. I. Lyapustin, S. Devadiga, C. Davidson and E. J. Masuoka (2013), Land and cryosphere products from Suomi NPP VIIRS: Overview and status. Journal of Geophysical Research: Atmospheres, Volume 118, Issue 17, Pages: 9753–9765, DOI: 10.1002/jgrd.50771

Kang, Daehyun; Im, Jungho; Lee, Myong-In; Quackenbush, Lindi J. (2014). The MODIS ice surface temperature product as an indicator of sea ice minimum over the Arctic Ocean. REMOTE SENSING OF ENVIRONMENT, 152, 99-108.

Key, J. R., R. Mahoney, Y. Liu, P. Romanov, M. Tschudi, I. Appel, J. Maslanik, D. Baldwin, X. Wang, and P. Meade (2013), Snow and ice products from Suomi NPP VIIRS, J. Geophys. Res. Atmos., 118, 12,816–12,830, doi:10.1002/2013JD020459.

Key, J., J. Collins, C. Fowler, and R. Stone (1997), High-latitude surface temperature estimates from thermal satellite data, Rem. Sens. Environ., 61, 302-309.

Key, J. and M. Haefliger (1992), Arctic ice surface temperature retrieval from AVHRR thermal channels, J. Geophys. Res., 97(D5), 5885-5893.

Krabill, W. B. and E. Buzay. 2012, updated 2014. IceBridge KT-19 IR Surface Temperature, Version 1. [2012-2015]. Boulder, Colorado USA. NASA National Snow and Ice Data Center Distributed Active Archive Center. http://dx.doi.org/10.5067/I883KXU7ZO8O.

Kurtz, N., J. Richter-Menge, S. Farrell, M. Studinger, J. Paden, J. Sonntag, and J. Yungel (2013), IceBridge Airborne Survey Data Support Arctic Sea Ice Predictions, Eos Transactions American Geophysical Union, 94(4), 41-41, http://dx.doi.org/10.1002/2013eo040001.

Kurtz, N.T., T. Markus, S.L. Farrell, D.L. Worthen (2011), Observations of recent Arctic sea ice thinning and its effect on ocean-atmosphere energy exchange and ice growth, J. Geophys. Res., 116, C04015, doi:10.1029/2010JC006235.

Lindsay, R.W. and D.A. Rothrock, (1994), Arctic sea ice surface temperature from AVHRR, Journal of Climate, 7 (1994), pp. 174–183.

Maslanik, J., J. Stroeve, C. Fowler, and W. Emery (2011), Distribution and trends in Arctic sea ice age through spring 2011, Geophys. Res. Lett., 38, L13502, doi: 10.1029/2011gl047735.

Maslanik, J.A., C. Fowler, J. Stroeve, S. Drobot, J. Zwally, D. Yi, and W. Emery (2007), A younger, thinner Arctic ice cover: Increased potential for rapid extensive sea-ice loss, Geophys. Res. Lett., VOL.34, L24501, doi:10.1029/2007GL032043.

Massom, R., and J.C. Comiso (1994), The classification of Arctic sea ice types and the determination of surface temperature using advanced very high resolution radiometer data, Journal Geophysical Research, 99(C3), pp 5201-5218.

Meier, W.N., G. Hovelsrud, B. van Oort, J. Key, K. Kovacs, C. Michel, M. Granskog, S. Gerland, D. Perovich, A.P. Makshtas, and J. Reist, 2014. Arctic sea ice in transformation: A review of recent observed changes and impacts on biology and human activity, Rev. Geophys., 52(3), doi:10.1002/2013RG000431.

NSIDC (2015), Arctic Sea Ice News and Analysis: 2015 Melt season in review, http://nsidc.org/arcticseaicenews/2015/10/2015-melt-season-in-review/.

Parkinson, C.L. and J.C. Comiso (2013), On the 2012 record low in Arctic sea ice cover: Combined impact of preconditioning and an August storm. Geophys. Res. Lett., 40, 1356-1361, doi: 10.1002/grl.50349.

Riggs, G. A., D. K. Hall, and S. A. Ackerman, (1999), "Sea ice extent and classification with the Moderate Resolution Imaging Spectroradiometer Airborne Simulator (MAS)." Remote Sensing of Environment, 68 (2): 152-163.

Tschudi, M.A., Fowler, C., Maslanik, J.A., and Stroeve, J., 2010. Tracking the movement and changing surface characteristics of Arctic sea ice. IEEE J. Selected Topics in Earth Obs. and Rem. Sens., 10.1109/JSTARS.2010.2048305.

Wang, X., J.R. Key, and Y. Liu (2010), A thermodynamic model for estimating sea and lake ice thickness with optical satellite data. Journal of Geophysical Research, Vol. 115, C12035, doi: 10.1029/2009JC005857.

Wang, X. and J. R. Key (2005), Arctic Surface, Cloud, and Radiation Properties Based on the AVHRR Polar Pathfinder Data Set. Part I: Spatial and Temporal Characteristics, J. Climate, Vol.18, No.14, 2558-2574.

Yu, Y., and R.W. Lindsay (2003), Comparison of thin ice thickness distributions derived from RADARSAT Geophysical Processor System and advanced very high resolution radiometer data sets, J. Geophys. Res., 108, 10.1029/2001JC000805.

Yu, Y. and D.A. Rothrock (1996), Thin ice thickness from satellite thermal imagery, J. Geophys. Res., Vol.101, No. C10, 25,753-25,766.

Yu, Y., A. Rothrock and R.W. Lindsay (1995), Accuracy of sea ice temperature derived from the advanced very high resolution radiometer, Journal of Geophysical Research, 100(C3), pp 4525-4532.